ARTICLES
PUBLISHED ONLINE: 28 FEBRUARY 2010 | DOI: 10.1038/NMAT2711
nature materials

Atomic layers of hybridized boron nitride and graphene domains

Lijie Ci[1†], Li Song[1†], Chuanhong Jin[2], Deep Jariwala[1‡], Dangxin Wu[3], Yongjie Li[1‡], Anchal Srivastava[1‡], Z. F. Wang[3], Kevin Storr[4], Luis Balicas[5], Feng Liu[3] and Pulickel M. Ajayan[1*]

Two-dimensional materials, such as graphene and monolayer hexagonal BN (*h*-BN), are attractive for demonstrating fundamental physics in materials and potential applications in next-generation electronics. Atomic sheets containing hybridized bonds involving elements B, N and C over wide compositional ranges could result in new materials with properties complementary to those of graphene and *h*-BN, enabling a rich variety of electronic structures, properties and applications. Here we report the synthesis and characterization of large-area atomic layers of *h*-BNC material, consisting of hybridized, randomly distributed domains of *h*-BN and C phases with compositions ranging from pure BN to pure graphene. Our studies reveal that their structural features and bandgap are distinct from those of graphene, doped graphene and *h*-BN. This new form of hybrid *h*-BNC material enables the development of bandgap-engineered applications in electronics and optics and properties that are distinct from those of graphene and *h*-BN.

Recent investigations have demonstrated that graphene has spectacular electronic properties[1]. Various approaches have been developed to fabricate high-performance graphene devices by engineering their bandgaps so as to improve their semiconducting properties. One of the most feasible methods to control the semiconducting properties of graphene is by doping, which is a process intentionally used to tailor the electrical properties of intrinsic semiconductors. Experimental and theoretical studies on graphene doping show the possibility of making p-type and n-type semiconducting graphene by substituting C atoms with B and N atoms[2–4], respectively. The dopant atoms can modify the electronic band structure of graphene, and open up an energy gap between the valence and conduction bands. More interestingly, B, C and N can be atomically mixed together to form various semiconducting hexagonal layered structures with varying stoichiometry, such as BCN nanotubes[5,6]. BCN graphitic films (thickness from 100 nm to a few micrometres) have been prepared by thermally decomposing B-, C- and N-containing precursors by chemical vapour deposition (CVD; ref. 7). Experimental studies and theoretical calculations have indicated that BCN nanostructures show semiconducting properties with a small bandgap[7–9] and interesting mechanical properties[10].

Previous studies have found that B–N and C–C bonds tend to segregate in the BCN systems[11]. For example, owing to their very similar lattice parameters, it is possible to synthesize layer-by-layer composite structures of hexagonal BN (*h*-BN) and graphene[12–14]. Theoretical calculations indicate that a small bandgap can be opened by placing a graphene layer onto an *h*-BN substrate[15]. A hybrid atomic monolayer consisting of hybridized phases of *h*-BN and graphene (*h*-BNC) is another interesting structure that would enable the tailoring of physical properties in graphene-based structures. *h*-BN is a material with a wide bandgap of up to 5.9 eV, with important applications as a deep-ultraviolet-light emitter[16,17]. We expect that the hybridized *h*-BNC structures would have interesting properties by combining the properties of two seemingly disparate materials with similar lattice parameters and crystal structure. Here we show that we have successfully synthesized uniform and continuous *h*-BNC films on a large area.

To synthesize *h*-BNC films, we used a thermal catalytic CVD method (see Supplementary Information for more details), which has the potential for large-wafer growth of graphene[18]. We chose Cu as substrate, which has been successfully used for large-area graphene growth[19]. Cu substrates have also been used previously for *h*-BN deposition[20]. A surface-adsorption growth mechanism has recently been proposed for graphene deposition on a Cu surface[21], implying that if we simultaneously supply a C and a BN source it may be possible to deposit two-dimensional (2D) monolayers of *h*-BNC. In our growth, methane and ammonia borane (NH_3–BH_3) were used as precursors for carbon and BN, respectively. The atomic ratio of B, C and N can be tuned by controlling the experimental parameters, although the B/N ratio is always unity. For example, we can control the atomic percentage of C from about 10% to ~100% (see Supplementary Table S1). After growth, the films were transferred to other substrates for further characterization (see Supplementary Fig. S1a,b). Similar to the processing of graphene, the *h*-BNC films could also be lithographically patterned and cut into various shapes by exposure in oxygen plasma (see Supplementary Fig. S1c). This enables *h*-BNC atomic films to be easily fabricated into devices. Figure 1a is a photograph of *h*-BNC film on a quartz substrate, showing that the film is transparent. Figure 1b shows an atomic force microscopy (AFM) image of the film on a Si substrate. Both optical

[1]Department of Mechanical Engineering & Materials Science, Rice University, Houston, Texas 77005, USA, [2]Nanotube Research Center, National Institute of Advanced Industrial Science and Technology (AIST), Tsukuba 305-8565, Japan, [3]Department of Materials Science & Engineering, University of Utah, Salt Lake City, Utah 84112, USA, [4]Department of Physics, Prairie View A&M University, Prairie View, Texas 77446, USA, [5]National High Magnetic Field Laboratory, Tallahassee, Florida 32310, USA. †These authors contributed equally to this work. ‡Present addresses: Department of Metallurgical Engineering, Banaras Hindu University, Varanasi 221005, India (D.J.); Department of Physics, Banaras Hindu University, Varanasi 221005, India (A.S.); Department of Chemistry, Lanzhou University, Lanzhou 730000, China (Y.L.). *e-mail: ajayan@rice.edu.

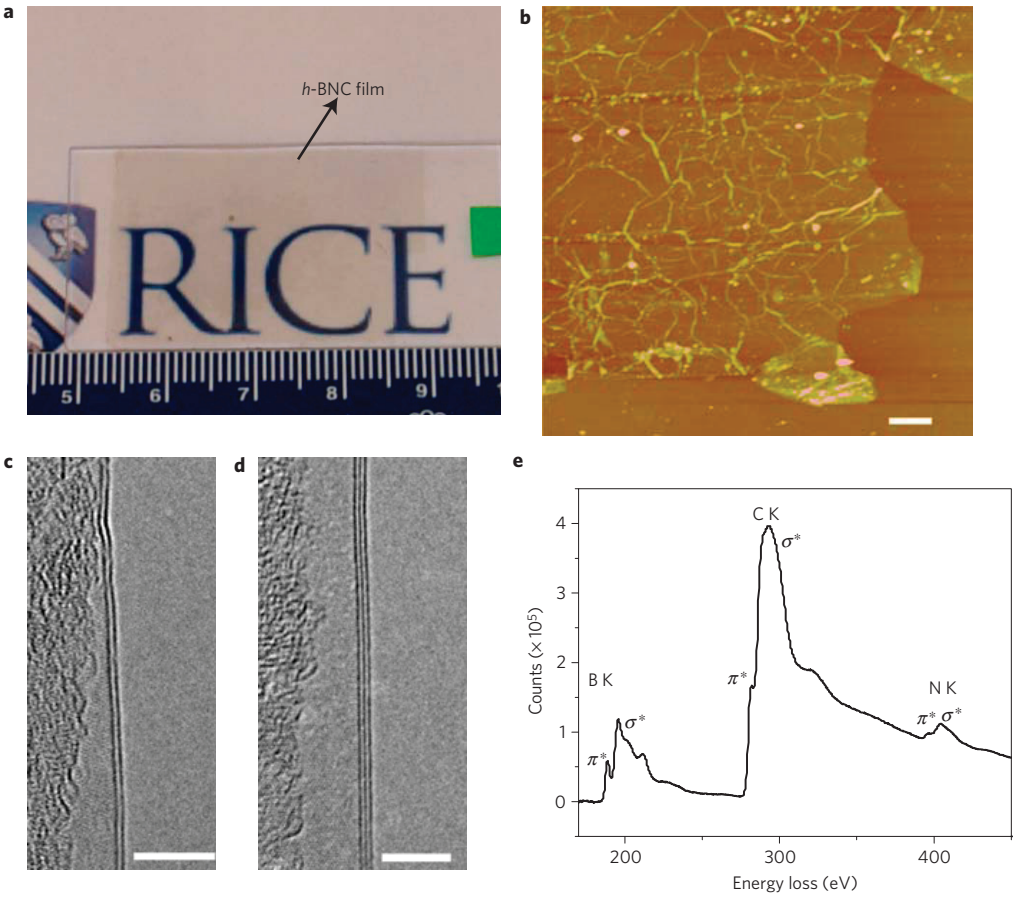

Figure 1 | Characteristics of an *h*-BNC film. a, Photograph of a transparent *h*-BNC film on a quartz slide. **b**, An AFM image shows the uniform thickness of an *h*-BNC film (scale bar: 1 μm). **c**,**d**, HRTEM images indicate that the as-grown films are two or three atomic layers thick (scale bars: 5 nm). **e**, K-shell excitations of B, C and N are revealed from the core EELS spectra taken from these films.

imaging and AFM images indicate that the film is fairly uniform except for some wrinkles. Further AFM thickness measurement indicates that the thickness of the films is about 1 nm (see Supplementary Fig. S2). High-resolution transmission electron microscopy (HRTEM) observations indicate that our *h*-BNC films mainly consist of two or three layers, as Fig. 1c,d shows. This is slightly different from the growth of graphene on Cu, which leads mainly to the growth of a single layer under similar conditions[19].

We made electron energy-loss spectroscopy (EELS) measurements on the *h*-BNC film to determine their chemical composition and structure. Figure 1e shows an EELS spectrum with three visible edges starting at 185, 276 and 393 eV, corresponding to the characteristic K-shell ionization edges of B, C and N, respectively[22]. The three bands corresponding to each element can be well resolved and show a first peak corresponding to the 1*s*-π^* antibonding orbit, followed by a wider band attributed to the 1*s*-σ^* antibonding orbit. This type of EELS edge structure proves that all three elements are sp^2 hybridized[22,23], and indicates that the atomic films grown on Cu possess a hexagonal structure consisting of B, C and N. Elemental mapping using energy filtered techniques (see Supplementary Fig. S3) also proves that all three elements are distributed over the entire area of the films. Using a low-voltage aberration-corrected HRTEM, we show the atomic structure of our as-grown *h*-BNC film (Fig. 2). As mentioned above, most of our *h*-BNC films are two or three layers thick. However, we can expose small areas showing projections from a single layer only (Fig. 2a), so that the atomic structure of an individual layer can be observed. The inset of Fig. 2a, showing the fast Fourier transform (FFT) from the image, indicates a hexagonal atomic structure. Even though individual atoms can be resolved from the hexagonal packing, we have not been able to identify the positions of the individual B, C and N atoms in the lattice, owing to their very close atomic sizes. Atomic HRTEM images and selected-area electron diffraction patterns taken from several areas show more details of our few-layer *h*-BNC films (see Supplementary Figs. S4,S5). We find that the multiple layers are typically in turbostratic stacking and that the different Moiré patterns seen in the atomic-scale images are due to the lack of AB stacking registry between the layers[24]. Figure 2b shows an image of such a Moiré pattern, and the FFT pattern shown in the inset shows three sets of hexagonal spots with a rotational angle of 11°, which indicates that this is a three-layer region, and the relative rotational angle with respect to each layer is 11°. Figure 2c shows an area with a different Moiré pattern, and the FFT pattern, as shown in the inset, indicates a two-layer stacking with a relative rotational angle of 16°. Using the FFT spots, we can reconstruct each sheet of the hexagonal atomic network, as shown in Fig. 2d,e (see Supplementary Fig. S6 for more details). The hexagonal atomic arrangement can be clearly identified from the reconstructed images. A proposed model for the structure of our atomic films based on hybridized domains of *h*-BN and C is shown in Fig. 2f. The model is based on our experimental analysis (the following sections and Supplementary Fig. S10 in Section S6) and theoretical calculations on the stability of *h*-BNC films (see more details in Supplementary Section S5).

Figure 3a–c shows an X-ray photoelectron spectroscopy (XPS) spectrum of B, N and C, respectively, from an as-grown *h*-BNC film. The shape and position of the spectra of all three elements are very different from those of previous XPS studies of films with BC_2N and BCN compositions[9,25]. The main peak of the B 1*s*

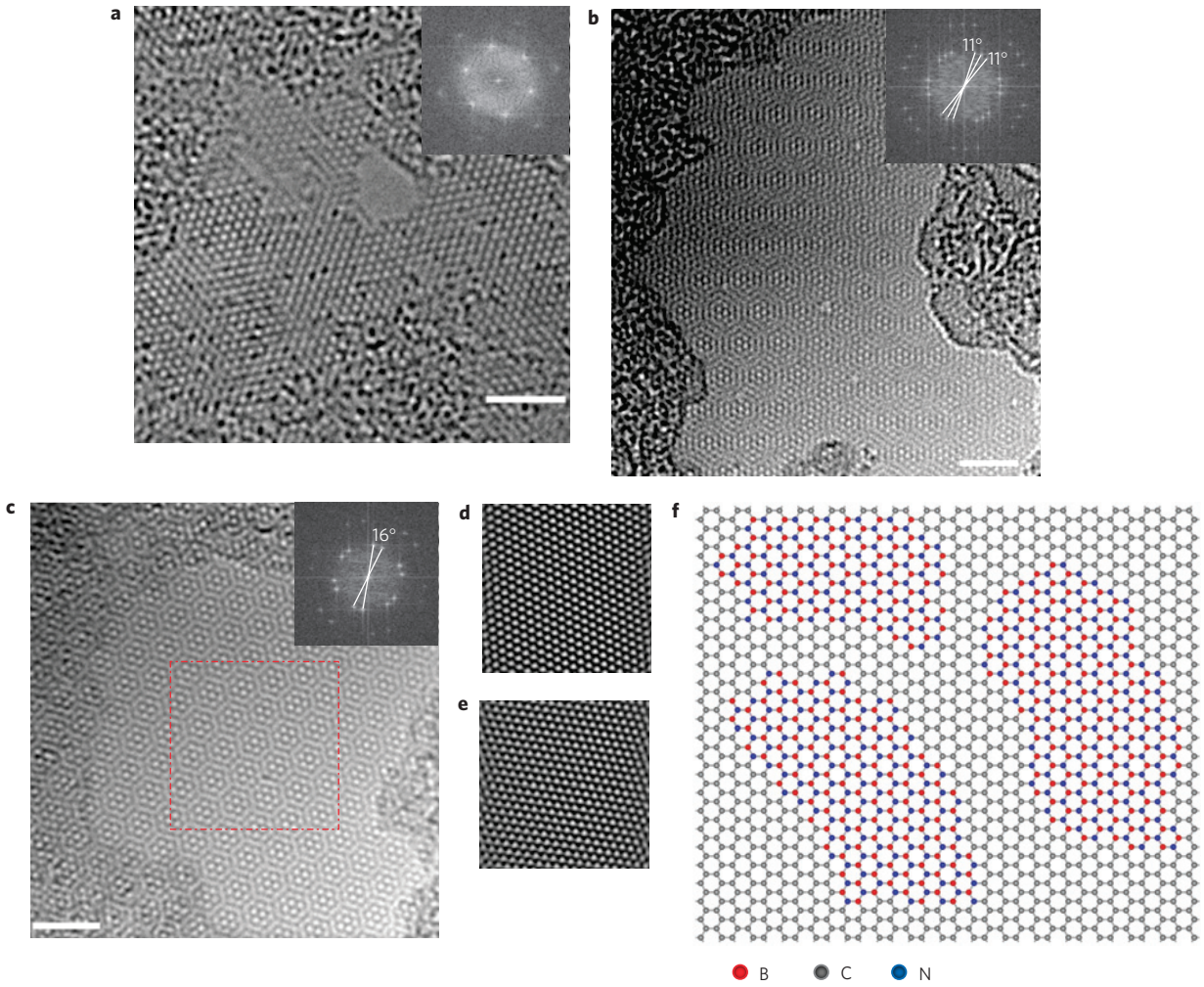

Figure 2 | Atomic HRTEM images of *h*-BNC film. a, An HRTEM image of a single-layer region exposed a nearby hole in the film. The inset is the FFT pattern of the single-layer region. **b**, An atomic-scale Moiré pattern; the inset FFT indicates a three-layer stacked region with rotational angle of 11°. **c**, A Moiré pattern from a different region; the FFT in the inset reveals a two-layer packing with a relative rotational angle of 16°. **d**,**e**, Two individual atomic layers reconstructed by masking the FFT pattern from the area in **c** (red line). **f**, Atomic model of the *h*-BNC film showing hybridized *h*-BN and graphene domains. Scale bars: 2 nm.

spectrum is at 190.9 eV (Fig. 3a), which is very close to that of B 1*s* (190.1 eV) in *h*-BN (ref. 9). This suggests that the main bonding configuration for B in our films is similar to that of *h*-BN, where three N atoms surround one B atom. However, a small shoulder at a lower binding energy of 188.4 eV implies a contribution from the bonding configurations of B and C, and this is because C atoms have a lower electronegativity than N (ref. 25). The N 1*s* peak is located at 398.0 eV (Fig. 3b), similar to the position of the N 1*s* spectrum (398.1 eV) of *h*-BN (ref. 9). However, the shoulder seen at the higher energies suggests that some N atoms partially bond with C atoms. Both the B 1*s* and the N 1*s* spectrum indicate that the main configuration for B and N atoms is the B–N bond, implying that *h*-BN domains exist in the film. The C 1*s* peak is located at 284.4 eV (Fig. 3c), which is close to the value observed in graphite (284.9 eV). This suggests that the C–C bonds stay together and form graphene domains. The small shoulder at the higher binding energies is due to C–N bonds, whereas the other one at lower binding energies is from C–B bonds. These bonds must be located at the boundaries of the hybridized *h*-BN and graphene domains, as shown in the atomic model in Fig. 2f.

Figure 3d shows a typical Raman spectrum of the *h*-BNC atomic film (top curve). Compared with that of a pure graphene sample (bottom curve), the *h*-BNC curve shows a much higher and broader D band at 1,360 cm^{-1}. At 1,620 cm^{-1} (D′ band), a shoulder appears on the right side of the G band. Both Raman D and D′ bands of carbon materials originate from the finite crystal size or lattice distortion[26]. The second-order Raman band located at about 2,700 cm^{-1} (2D band) has been used to determine the number of layers of CVD-grown graphene according to its relative intensity with respect to the G band and its position[18,19]. The intensity of the 2D band from the pure graphene is about twice that of the G band, indicating one to two layers of graphene. For bilayer or trilayer pure graphene, the intensity of the 2D band is supposed to be equal to that of the G band. However, in the *h*-BNC film (2–3 layers), the intensity of the 2D band is suppressed, possibly owing to a strong photoluminescence background. Our Raman data support the model of domain structure (Fig. 2f) in our *h*-BNC films. For example, if they were *h*-BN/graphene stacked structures, as we did not see apparent Raman signal from our CVD-grown pure BN, the Raman spectrum should be very close to that of graphene. We should observe a lower D peak at 1,340 cm^{-1} and a higher and narrower G peak at 1,580 cm^{-1}, and a 2D peak at around 2,700 cm^{-1} should provide us with information about the formation of single- or bilayer graphene. Experimentally, we can tune the compositional ranges of the two components (C and BN) over the whole range, a fact that also does not support a BN/graphene stacked structure (for

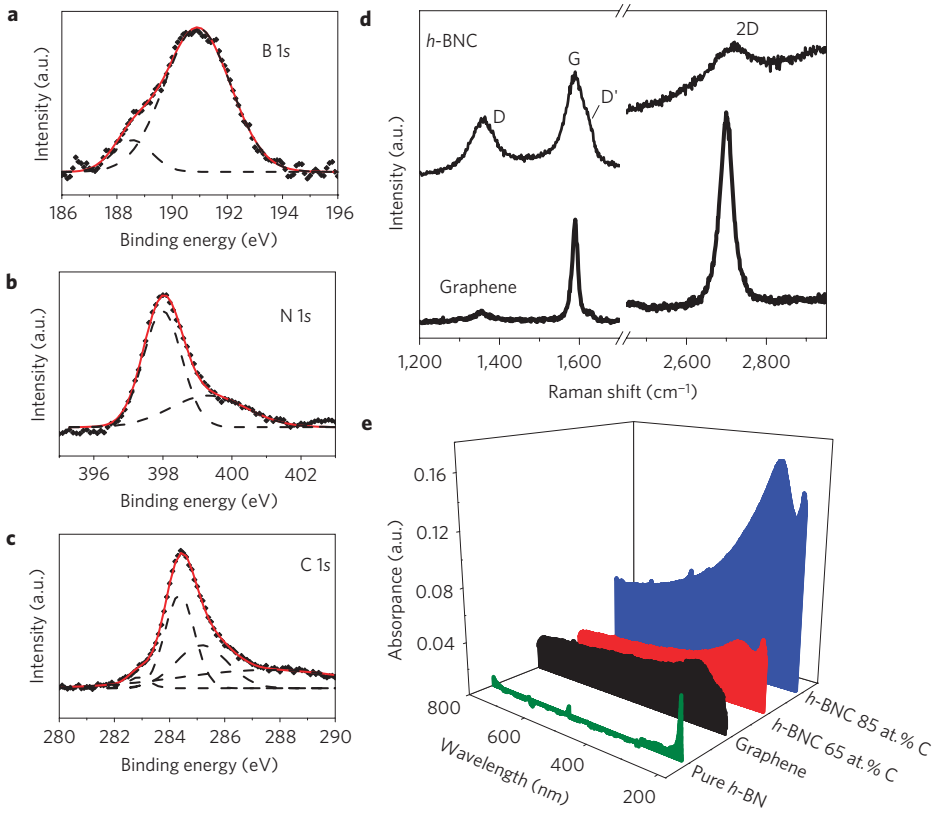

Figure 3 | Evidence for hybridized *h*-BN and graphene domain-like structure of *h*-BNC. a–c, XPS spectra of B, N and C 1*s* core levels, respectively. The spectrum curves (filled diamonds) are deconvoluted (black dashed curves) by Gaussian fitting (red curves), indicating possible multibonding information. **d**, Raman spectrum of an *h*-BNC and a CVD-grown graphene film. **e**, Ultraviolet–visible absorption spectra of different graphene films.

example, a two-layer film should be restricted to 50 at.% carbon). We can conclude that both Raman D and D′ bands should be mainly attributed to disorders and boundaries in the carbon network induced by BN domains.

The ultraviolet–visible absorption spectrum was taken to investigate the optical energy gap of the *h*-BNC film owing to optically induced transitions. The optical bandgaps are determined on the basis of Tauc's formulation[27]. As Fig. 3e shows, a graphene sample shows a very weak absorption edge in the range of 190–800 nm. The absorption spectrum of the *h*-BN sample shows one absorption edge at 218 nm, which corresponds to an optical bandgap of 5.69 eV (see Supplementary Fig. S7 for the method). Absorption curves from *h*-BNC films show two absorption edges, indicating two possible domain structures as proposed. For the *h*-BNC sample with 65 at.% C, the first absorption edge corresponds to an optical bandgap of 4.48 eV, which must come from *h*-BN domains in the film. However, it is smaller than that of *h*-BN sample (5.69 eV), indicating the effect of C doping. There may be some intrinsic doping (C atom in BN or B, N in graphene domain) or a boundary effect, which are difficult to distinguish from each other. We can see that increasing C content to 84 at.% lowers this value to 3.85 eV. The second absorption edge corresponds to an optical bandgap of 1.62 eV and 1.51 eV from the samples with 65 at.% C and 84 at.% C, respectively. This absorption edge must be from *h*-BN-doped graphene domains. On the basis of the measured bandgaps, we expect the domain size to be larger than a few nanometres (see Supplementary S6). If all the domain sizes were smaller than 2–3 nm, then the film would behave like a BN–C 'alloy', with a bandgap equal to the average gap of *h*-BN and graphene, similar to the case of a short-period semiconductor superlattice[28]. The fact that we observe two different optical bandgaps indicates that both the *h*-BN and graphene domains are large enough to resume their individual bandgap identities, forming effectively a superlattice. This provides further evidence that the film we have made consists of hybrid atomic layers of *h*-BN and C graphene nanodomains rather than a substitutionally doped (B and N in C) or alloyed phase between *h*-BN and pure graphene.

To investigate electrical properties of the *h*-BNC films, devices with four electrodes were fabricated (see Fig. 4a, and also Supplementary Fig. S8a,b). Figure 4b shows the linear *I*–*V* behaviour from all the samples. We found that the electrical conductivity of *h*-BNC ribbon increases on increasing its percentage of carbon. The pure BN film is an insulator, whereas the *h*-BNC ribbon with 94% carbon has a lower resistivity, around $10^{-3}\ \Omega$ cm. This suggests that we can easily control the electrical properties of our *h*-BNC films from insulator to highly conducting by tuning the carbon concentration. Figure 4c shows the back-gate-dependent electrical response of an *h*-BNC sample (40 at.% C) at room temperature. The drain current is modulated by applying a gate voltage. Our *h*-BNC field-effect transistor shows an ambipolar semiconducting behaviour, which is similar to that of CVD-grown graphene[17–19]. This result further indicates that our films have an atomic structure consisting of hybridized *h*-BN and graphene domains, because theoretical and experimental investigations have indicated that B, C, N mixed atomic structures are typically p-type semiconductors[29,30]. The *h*-BN domains decrease the gating effect, which results in a lower effective gate modulation behaviour. We calculate the carrier mobility from the slope of the conductivity variation with gate voltage. The electron and hole mobility of our *h*-BNC devices is in the range of 5–20 $cm^2\ V^{-1}\ s^{-1}$. This value is much smaller than the mobilities reported for graphene[17,19], and can be attributed to electron scattering at the boundaries between *h*-BN and graphene domains inside the sample. The carrier scattering also induces a charge-neutrality point (point of

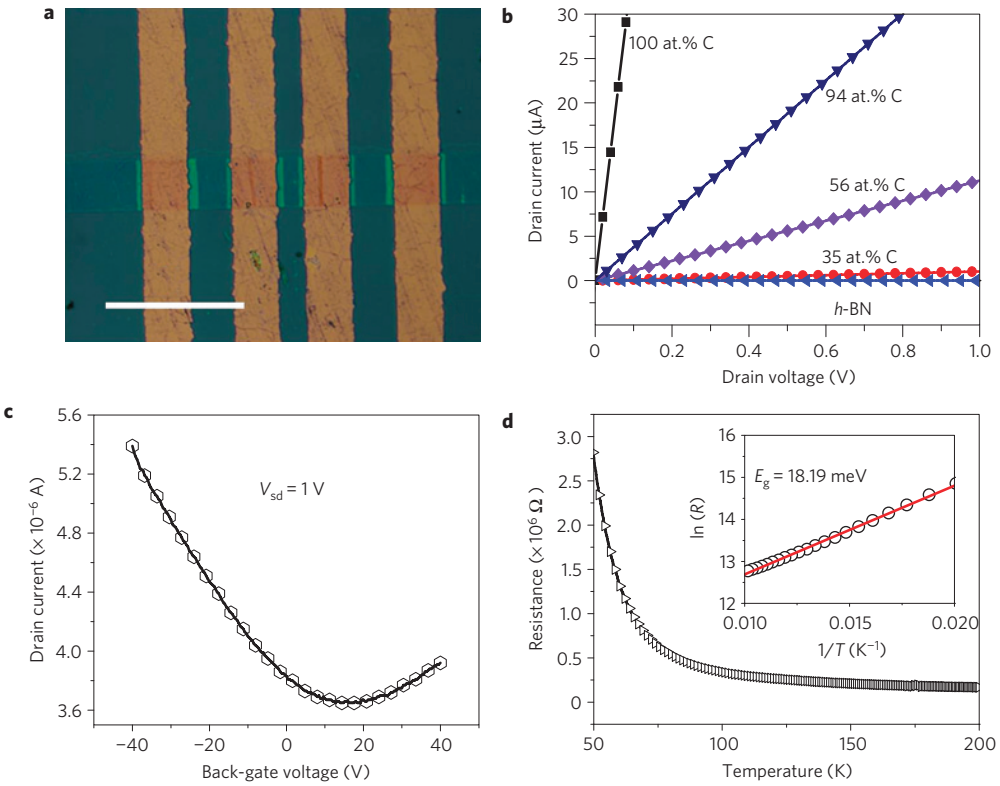

Figure 4 | Electrical properties of *h*-BNC atomic films. a, Optical image of a four-terminal *h*-BNC ribbon field-effect transistor. Scale bar: 30 μm. **b**, Current–voltage (I–V) characteristics of as-grown BNC with different percentages in carbon measured at room temperature. **c**, The drain current as a function of the voltage applied to the back gate for a 7-μm-wide BNC ribbon with 40% carbon. The drain–source voltage is fixed to 1 V. **d**, A resistance-versus-temperature curve for a typical *h*-BNC ribbon with a width of 5 μm and a length of 11 μm. The inset shows ln(R) as a function of T^{-1} in the temperature range from 50 to 100 K. The linear fit (solid line) shows that the data are well described by $R(T) \propto \exp(E_\Delta/k_B T)$. E_Δ is the bandgap and k_B is Boltzmann's constant.

minimum conductivity) shifting up to a gate voltage of 18 V (ref. 31) (see Supplementary Fig. S8c for more neutrality-point shifts at various carbon percentages). We would like to point out here that the above electrical transport data do not support a C/BN stacked structure: otherwise, the conductivity should be dominated by the highly conducting graphene layer.

Temperature-dependent electrical transport measurements on our *h*-BNC samples (Fig. 4d) show a significant increase in the resistance by more than 10-fold on cooling down from room temperature to 50 K, which is a typical semiconducting behaviour. The value of the bandgap is calculated on the basis of a linear Arrhenius plot of the logarithm of the resistance ln(R) versus the inverse temperature T^{-1} (see Fig. 4d, inset). The measured bandgap is 18 meV for a 5-μm-wide *h*-BNC ribbon with 56 at.% carbon, and this value for the bandgap is close to that of a 30-nm-wide pristine graphene ribbon[32]. As discussed above, the *h*-BNC samples consist of a percolating graphene network embedded with BN domains. As the BN domains have a very large bandgap (~5 eV) acting like an 'infinite' barrier, the electronic and transport properties of the graphene network will be similar to those of the graphene nanohole superlattices[33]. Small gaps are opened in the graphene owing to quantum confinement and/or spin polarization at specific C–BN boundaries (see Supplementary Fig. S9c).

First-principles calculations on the basis of the density functional theory were carried out to model the *h*-BNC structure. Our modelling results, as well as recent reports[34], indicate that BN and C are thermodynamically immiscible, preferring to separate into 2D domains in planar *h*-BNC structures. However, our calculations also indicate that larger domains would be preferred to decrease the total domain interfacial energy in the system (see Supplementary Fig. S9a,b). Using the tight-binding method, we estimated an upper limit of the domain size for the film with 50 at.% C to be ~42 nm from the measured gap of 18 meV (see Supplementary Fig. S9c). Our modelling indicates that the experimentally observed *h*-BNC must be a kinetically stabilized non-equilibrium-grown structure where the actual domain size could be controlled by various kinetic factors, such as the growth temperature, the deposition rate and the effect of the substrate.

We have synthesized a new form of 2D atomic film consisting of hybridized *h*-BN and C (graphene) domains, showing structural features and a bandgap that have not been found in graphene, *h*-BN or boron- and nitrogen-codoped graphene. This new structure with separated graphene and BN domains and a wide range of compositions may be engineered to build unique semiconducting 2D architectures, which could have potential applications in electronics and optics. These hybridized atomic films are an isotropic structure, and we did not observe any anisotropic property in our electrical transport or optical results. In addition, the *h*-BN domains can act as long-range impurities within the graphene lattice, making *h*-BNC a promising system for fundamental physical investigations, such as charge localization[35] and possible metal–insulator transitions[36].

Methods

CVD growth process. Growth of boron-nitride-hybridized graphene (*h*-BNC) was carried out in a split tube furnace with a fused-quartz processing tube (50 mm outer diameter). Boron and nitrogen were introduced into the system by separately heating ammonia borane using a heating belt in the front region of the processing tube. The Cu substrate was placed in the furnace under vacuum, annealed at 600 °C for 20 min in Ar/H_2 (15 vol% H_2) flow and gradually heated up to 900–1,000 °C in 40 min. Methane and ammonia borane were then introduced into the growth chamber. During the growth process, Ar/H_2 flow was shut down, and the system

vacuum was controlled by the methane flow (about 200 mtorr). The growth of pure *h*-BN and graphene films was also carried out without methane flow and BN introduction, respectively.

Characterization methods. HRTEM, selected-area electron diffraction, EELS measurements and elemental mapping (Gatan GIF) were carried out on a JEOL-2100 field emission HRTEM operated at 200 kV. Atomically resolved HRTEM observations were conducted within a TEM set-up (JEOL-2010F, operated at 120 and 80 kV) equipped with a postspecimen aberration corrector (CEOS). XPS (PHI Quantera XPS) was carried out using monochromatic aluminium Kα X-rays. XPS data were analysed with the MultiPak software. Raman spectroscopy (Renishaw inVia) was used to characterize the structure of the film at 514.5 nm laser excitation. Optical-absorptance measurements (Shimadzu ultraviolet-3600) were made on atomic films after they were transferred onto optical quartz plates. The as-grown *h*-BNC film was transferred onto an n-type silicon wafer with a 300-nm-thick SiO_2 layer for the fabrication of a back-gated field-effect transistor. Optical lithography and the oxygen-plasma-etching process were used to pattern the thin film into long *h*-BNC ribbons with widths ranging from 5 to 15 µm. Electrodes (Au/Ti = 30 nm/3 nm) were patterned onto the *h*-BNC ribbon by using optical lithography and e-beam evaporator techniques. A probe station was used to test the electrical properties of *h*-BNC at room temperature. All of the reported electrical transport measurements were made in a 10^{-5} torr vacuum chamber. We further characterized the electrical properties of *h*-BNC ribbon by investigating the temperature dependence of the resistance in a ^{3}He cryostat. The data were recorded by using a Lakeshore resistance bridge in a four-terminal configuration.

Received 21 October 2009; accepted 27 January 2010; published online 28 February 2010

References

1. Geim, A. K. & Novoselov, K. S. The rise of graphene. *Nature Mater.* **6,** 183–191 (2007).
2. Wang, X. *et al.* N-doping of graphene through electrothermal reactions with ammonia. *Science* **324,** 768–771 (2009).
3. Martins, T. B., Miwa, R. H., da Silva, A. J. R. & Fazzio, A. Electronic and transport properties of boron-doped graphene nanoribbons. *Phys. Rev. Lett.* **98,** 196803 (2007).
4. Lherbie, A., Blasé, R. X., Niquet, Y., Triozon, F. & Roche, S. Charge transport in chemically doped 2D graphene. *Phys. Rev. Lett.* **101,** 036808 (2008).
5. Cherrey, K. *et al.* Synthesis of $B_xC_yN_z$ nanotubules. *Phys. Rev. B* **51,** 11229–11232 (1995).
6. Golberg, D., Dorozhkin, P., Bando, Y. & Dong, Z. C. Synthesis, analysis and electrical property measurements of compounds nanotubes in the ceramic B–C–N system. *MRS Bull.* **29,** 38–42 (2004).
7. Kaner, R. B., Kouvetakis, J., Warble, C. E., Sattler, M. L. & Bartlett, N. Boron–carbon–nitrogen materials of graphite-like structure. *Mater. Res. Bull.* **22,** 399–404 (1987).
8. Liu, A. Y., Wentzcovitch, R. M. & Cohen, M. L. Atomic arrangement and electronic structure of BC_2N. *Phys. Rev. B* **39,** 1760–1765 (1989).
9. Miyamoto, Y., Rubio, A., Cohen, M. L. & Louie, S. G. Chiral tubules of hexagonal BC_2N. *Phys. Rev. B* **50,** 4976–4979 (1994).
10. Hernández, E., Goze, C., Bernier, P. & Rubio, A. Elastic properties of C and $B_xC_yN_z$ composite nanotubes. *Phys. Rev. Lett.* **80,** 4502–4505 (1998).
11. Kawaguchi, M., Kawashima, T. & Nakajima, T. Syntheses and structures of new graphite-like materials of composition BCN(h) and BC_2N(H). *Chem. Mater.* **8,** 1197–1201 (1996).
12. Suenaga, K. *et al.* Synthesis of nanoparticles and nanotubes with well-separated layers of boron nitride and carbon. *Science* **278,** 653–655 (1997).
13. Han, W. Q., Mickelson, W., Cumings, J. & Zettl, A. Transformation of $B_xC_yN_z$ nanotubes to pure BN nanotubes. *Appl. Phys. Lett.* **81,** 1110–1112 (2002).
14. Kawasaki, T. *et al.* Double atomic layers of graphene/monolayer *h*-BN on Ni(111) studied by scanning tunnelling microscopy and scanning tunnelling spectroscopy. *Surf. Rev. Lett.* **9,** 1459–1464 (2002).
15. Giovannetti, G., Khomyakov, P. A., Brocks, G., Kelly, P. J. & van den Brink, J. Substrate-induced band gap in graphene on hexagonal boron nitride: *Ab initio* density functional calculations. *Phys. Rev. B* **76,** 073103 (2007).
16. Watanabe, K., Taniguchi, T. & Kanda, H. Direct-band gap properties and evidence for ultraviolet lasing of hexagonal boron nitride single crystal. *Nature Mater.* **3,** 404–409 (2004).
17. Kubota, Y., Watanabe, K., Tsuda, O. & Taniguchi, T. Deep ultraviolet light–emitting hexagonal boron nitride synthesized at atmospheric pressure. *Science* **317,** 932–934 (2007).
18. Reina, A. *et al.* Large area, few-layer graphene films on arbitrary substrates by chemical vapour deposition. *Nano Lett.* **9,** 30–35 (2009).
19. Li, X. *et al.* Large-area synthesis of high-quality and uniform graphene films on copper foils. *Science* **324,** 1312–1314 (2009).
20. Preobrajenski, A. B., Vinogradov, A. S. & Mårtensson, N. Monolayer of *h*-BN chemisorbed on Cu(111) and Ni(111). *Surf. Sci.* **582,** 21–30 (2005).
21. Li, X., Cai, W., Colombo, L. & Ruoff, R. S. Evolution of graphene growth on Cu and Ni studied by carbon isotope labeling. *Nano Lett.* **9,** 4268–4272 (2009).
22. Stephan, O. *et al.* Doping graphitic and carbon nanotube structures with boron and nitrogen. *Science* **266,** 1683–1685 (1994).
23. Kouvetakis, J. *et al.* Novel aspects of graphite intercalation by fluorine and fluorides and new B/C, C/N and B/C/N materials based on the graphite network. *Synth. Met.* **34,** 1–7 (1989).
24. Warne, J. H., Rümmeli, M. H., Gemming, T., Büchner, B. & Briggs, G. A. D. Direct imaging of rotational stacking faults in few layer graphene. *Nano Lett.* **9,** 102–106 (2009).
25. Watanabe, M. O., Itoh, S., Mizushima, K. & Sasaki, T. Bonding characterization of BC_2N thin films. *Appl. Phys. Lett.* **68,** 2962–2964 (1996).
26. Pimenta, M. A. *et al.* Studying disorder in graphite-based systems by Raman spectroscopy. *Phys. Chem. Chem. Phys.* **9,** 1276–1291 (2007).
27. Tauc, J., Grigorovici, R. & Vancu, A. Optical properties and electronic structure of amorphous germanium. *Phys. Status Solidi* **15,** 627–637 (1966).
28. Ihm, J. Effects of the layer thickness on the electronic character in GaAs–AlAs superlattices. *Appl. Phys. Lett.* **50,** 1068–1070 (1987).
29. Watanabe, M. O., Itoh, S., Mizushima, K. & Sasaki, T. Electrical properties of BC_2N thin films prepared by chemical vapour deposition. *J. Appl. Phys.* **78,** 2880–2882 (1995).
30. Watanabe, M. O., Itoh, S., Sasaki, T. & Mizushima, K. Visible-light-emitting layered BC2N semiconductor. *Phys. Rev. Lett.* **77,** 187–189 (1996).
31. Novoselov, K. S. *et al.* Electric field effect in atomically thin carbon films. *Science* **306,** 666–669 (2004).
32. Han, M. Y., Özyilmaz, B., Zhang, Y. & Kim, P. Energy band-gap engineering of graphene nanoribbons. *Phys. Rev. Lett.* **98,** 206805 (2007).
33. Liu, W., Wang, Z. F., Shi, Q. W., Yang, J. & Liu, F. Band gap scaling of graphene nanohole superlattices. *Phys. Rev. B* **80,** 233405 (2009).
34. Yuge, K. Phase stability of boron carbon nitride in a heterographene structure. *Phys. Rev. B* **79,** 144109 (2009).
35. Carroll, D. L. Effects of nanodomain formation on the electronic structure of doped carbon nanotubes. *Phys. Rev. Lett.* **81,** 2332–2335 (1998).
36. Zhang, Y. *et al.* Localization and the Kosterlitz–Thouless transition in disordered graphene. *Phys. Rev. Lett.* **102,** 106401 (2009).

Acknowledgements

P.M.A. acknowledges support from Rice University start-up funds and funding support from the Office of Naval Research (ONR) through the MURI programme on graphene and the Basic Energy Sciences division of the Department of Energy (DOE). L.C. (for work carried out on graphene growth and structural characterization) was supported by the ONR MURI programme (award No N00014-09-1-1066) and L.S. (for work done in device fabrication and electrical characterization) by DOE-BES programme DE-SC0001479. C.J. acknowledges the International Balzan Foundation for financial support through Meijo University. F.L. acknowledges support from DOE-BES programme DE-FG0203ER46027. Y.L. acknowledges a scholarship from the Chinese State Scholarship fund. A.S. acknowledges support from the BOYSCAST scheme sponsored by the Department of Science and Technology (DST), India. K.S. acknowledges support from the National Science Foundation Major Research Instrumentation programme (NSF-MRI) DMR-0619801 (for the dilution refrigerator) and the Department of Energy National Nuclear Security Administration (DOE-NNSA) DE-FG52-05NA27036 (17 T magnet and ^{3}He system) and the PVAMU Title III Program US Department of Education (infrastructure). L.B. acknowledges support from DOE-BES and NHMFL-UCGP programmes.

Author contributions

L.C. and L.S. contributed equally to this work. L.C. and L.S. designed and carried out most of the experiments (CVD, TEM, AFM, XPS, Raman, ultraviolet–visible spectra, electrical test), and analysed the data. C.J. carried out atomically resolved HRTEM work. D.J. and A.S. conducted part of the CVD growth. Y.L. conducted part of the XPS measurement. K.S., L.B. and L.S. conducted electrical measurements and data analysis. D.W., Z.F.W. and F.L. carried out the modelling. P.M.A was responsible for the project planning. L.C., L.S., P.M.A. and F.L. co-wrote the paper. All the authors discussed the results.

Additional information

The authors declare no competing financial interests. Supplementary information accompanies this paper on www.nature.com/naturematerials. Reprints and permissions information is available online at http://npg.nature.com/reprintsandpermissions. Correspondence and requests for materials should be addressed to P.M.A.